EDGE ARTICLE

Penetration depth tunable BODIPY derivatives for pH triggered enhanced photothermal/photodynamic synergistic therapy†

Jianhua Zou,[a] Peng Wang,[a] Ya Wang,[a] Gongyuan Liu,[a] Yewei Zhang,[d] Qi Zhang,[c] Jinjun Shao, [ID][a] Weili Si, [ID] *[a] Wei Huang [ID][b] and Xiaochen Dong [ID] *[a]

Improving the deep-tissue phototherapy (PDT) efficiency in the near-infrared (NIR) region has become one of the major challenges in clinics for cancer treatment. Developing intelligent photosensitizers (PSs) responding to tumor-specific signals sensitively to minimize side effects is another major challenge for tumor phototherapy. Herein, three phenyl-based boron dipyrromethene (BODIPY) compounds with different numbers of diethylaminophenyl groups introduced onto the BODIPY core have been designed and synthesized by the Knoevenagel condensation reaction. The absorbance of these compounds (BDPmPh, BDPbiPh, and BDPtriPh) can be controlled easily for realizing the tunable penetration depth. Moreover, the diethylamino groups in these designed PSs can serve as proton acceptors triggered by the low pH in lysosomes which can enhance the efficacy of photodynamic and photothermal therapy. The corresponding nanoparticles (NPs) of the compounds are prepared through a nanoprecipitation method and *in vitro* studies demonstrate that the ultra-low drug dosage of BDPtriPh NPs (half-maximal inhibitory concentration, $IC_{50} = 4.16$ μM) is much lower than that of BDPmPh NPs (50.09 μM) and BDPbiPh NPs (22.4 μM). *In vivo* fluorescence imaging shows that these NPs can be passively targeted to tumors by the enhanced permeability and retention (EPR) effect, and BDPtriPh NPs exhibit the fastest accumulation (about 4 hours). *In vivo* phototherapy indicates that BDPtriPh NPs with the longest NIR absorbance (813 nm) and highest photothermal conversion efficiency (60.5%) can effectively inhibit tumor growth and reduce side effects to normal tissues. This study provides a strategy to modulate the photoconversion characteristics of PSs for both penetration-depth-tunable and pH-dependent PDT/PTT synergistic cancer therapy in clinics.

Introduction

Effective new cancer treatments to replace or complement traditional therapeutic methodologies such as surgery, radiotherapy, and chemotherapy are urgently needed due to the fact that cancer is now the second leading cause of death globally.[1] To design and prepare theranostic agents on a single platform for both diagnosis and therapy is a promising research direction because traditional therapies suffer from lack of targeting, invasion and side effects.[2–5] Photodynamic therapy (PDT)

[a]*Key Laboratory of Flexible Electronics (KLOFE), Institute of Advanced Materials (IAM), Nanjing Tech University (Nanjing Tech), 30 South Puzhu Road, Nanjing, 211800, China. E-mail: iamxcdong@njtech.edu.cn; iamwlsi@njtech.edu.cn*

[b]*Shaanxi Institute of Flexible Electronics (SIFE), Northwestern Polytechnical University (NPU), 127 West Youyi Road, Xi'an 710072, China*

[c]*School of Pharmaceutical Sciences, Nanjing Tech University (Nanjing Tech), 30 South Puzhu Road, Nanjing 211800, China*

[d]*Department of Hepatobiliary and Pancreatic Surgery, Zhongda Hospital, Medical School, Southeast University, Nanjing 210009, China*

† Electronic supplementary information (ESI) available. See DOI: 10.1039/c8sc02443j

usually depends on non-toxic photosensitizers (PSs) to transfer absorbed photon energy to triplet oxygen ($^3O_2$) and generate toxic singlet oxygen ($^1O_2$) to kill cancer cells.[6–17] In addition, the fluorescence of the PSs can be further employed for fluorescence imaging. So far, a number of PSs have been applied for PDT, such as quantum dots, upconversion nanoparticles and organic nanoparticles.[18–27] Despite the advantages of PDT, the phototherapy efficacy is far from satisfactory. For instance, the limited tissue penetration depth may decrease the efficacy.

Photothermal therapy (PTT) utilizes near infrared (NIR) photothermal agents to convert the energy in light to heat at the target site. So far, a number of photothermal agents, including inorganic nanomaterials (such as carbon nanotubes and nanogold) and organic NIR dyes (such as indocyanine green (ICG)) have been reported.[28–32] From the viewpoint of synergistic therapy, combining PDT with PTT is an effective strategy to maximize efficacy and minimize side effects. However, these reported agents can only achieve single modality therapy or imaging, which is disadvantageous for synergistic therapy. Besides, some commercial photosensitizers, such as ICG, may suffer from photo-bleaching. An ideal photosensitizer

preferably possesses the following advantage: NIR absorbance is preferred since it allows an outstanding penetration depth in deep cancer tissues with targeting ability towards tumors; thus side effects to normal tissues can be minimized. On the other hand, due to the acidity of lysosomes, it is better to introduce some functional groups that are activable in this environment into the nanotheranostic system to obtain enhanced photo-therapy efficacy. BODIPY derivatives are widely acknowledged as excellent candidates due to their advantages such as high fluorescence, anti-photobleaching property, *etc.* For example, Han *et al.* reported NIR photosensitized nanoparticles for enhanced photodynamic therapy through resonance energy transfer.[33] In another example, Chen *et al.* reported a photo-conversion tunable fluorophore for wavelength dependent photoinduced cancer therapy.[34]

Inspired by these observations, three BODIPY derivatives (BDPmPh, BDPbiPh and BDPtriPh) with NIR absorbance have been designed and prepared by the Knoevenagel condensation reaction and introduced with diethylamino groups onto the BODIPY core. By conjugating different numbers of diethylamino groups, BODIPY derivatives with higher NIR absorbance (BDPmPh, BDPbiPh and BDPtriPh) are obtained, indicating their potential for adjustable tissue penetration.

Singlet oxygen generation and photothermal conversion ability measured under different pH suggest that enhanced photodynamic and photothermal efficacy could be obtained with the diethylamino groups as the proton acceptor. To improve dispersity in water, nanoparticles of the three compounds are prepared by nano-precipitation. An *in vitro* study on HeLa cells demonstrates that BDPmPh, BDPbiPh and BDPtriPh NPs possess a decreased half-maximal inhibitory concentration (IC_{50}) under irradiation but their dark toxicity can be ignored. A sub-cellular co-localization study indicates that they can target the lysosomes well, promising an enhanced performance of synergistic PDT and PTT. *In vivo* fluorescence imaging shows that these NPs can target tumors by an enhanced permeability and retention (EPR) effect and BDPtriPh NPs can accumulate at tumor sites only 4 h after intravenous injection, which is superior to that of BDPmPh NPs (8 h) or BDPbiPh NPs (6 h). This may be attributed to the fact that BDPtriPh NPs with the most diethylamino groups are able to accept more protons. Although all these NPs can inhibit the growth of tumors, BDPtriPh NPs are the best. In addition, no obvious damage was observed in normal tissues, including the heart, liver, lungs, spleen and kidneys, suggesting low dark toxicity as well as excellent bio-compatibility. This work introduces a new strategy to extend and enhance phototherapy by molecular design for wavelength as well as pH dependent synergistic PDT/PTT.

Experimental

Materials and apparatus

General chemicals were purchased from Sigma (Shanghai, Co. Ltd) and used without further purification. ^{1}H NMR and ^{13}C NMR spectra were measured on a Bruker DRX NMR spectrometer at 298 K in a $CDCl_3$ solution with residual solvent as the internal standard. UV-vis spectra were measured on a UV-3600 spectrophotometer (Shimadzu, Japan). Fluorescence spectra were recorded on an F-4600 HITACHI spectrophotometer from Japan. DLS was carried out on a 90 Plus particle size analyzer (Brookhaven Instruments, USA). TEM of the nanoparticles was performed on JEOL JEM-2100 equipment. Fluorescence bio-imaging of tumors and the main organs (heart, liver, spleen, lungs and kidneys) was performed on a PerkinElmer IVIS Lumina K.

Synthesis of BDPmPh, BDPbiPh and BDPtriPh

BDP (5,5-difluoro-1,3,7,9-tetramethyl-10-phenyl-5*H*-dipyrrolo [1,2-*c*:2′,1′-*f*][1,3,2]diazaborinin-4-ium-5-uide) (0.324 g, 0.1 mmol) and 4-(diethylamino)benzaldehyde (0.389 g, 0.22 mmol) were added into 15 mL *N,N*-dimethylformamide under a N_2 atmosphere. The system was heated to 100 °C, and acetic acid (0.4 mL) and piperidine (0.4 mL) were added. After 4 h, the mixture was poured into 150 mL water and extracted with dichloromethane. The organic layer was washed with brine and dried with anhydrous sodium sulfate. The solvent was removed by rotary evaporation, and the crude product was purified by column chromatography (silica gel, DCM : PE = 1 : 2, v/v). Yield: 55%, ^{1}H NMR ($CDCl_3$, 400 MHz): δ (ppm) 7.48–7.44 (m, 6H), 7.34–7.28 (m, 2H), 7.20 (d, J = 16.4 Hz, 1H), 6.65–6.59 (m, 3H), 5.96 (s, 1H), 3.40 (q, J = 7.2 Hz, 4H), 2.56 (s, 3H), 1.41–1.37 (m, 6H), 1.19 (t, J = 7.7 Hz, 6H). ^{13}C NMR (75 MHz, $CDCl_3$): δ (ppm) 148.6, 142.9, 140.5, 138.0, 135.5, 131.8, 129.6, 128.9, 128.7, 128.5, 128.3, 124.5, 124.0, 123.8, 120.3, 119.9, 119.1, 117.7, 115.6, 113.9, 111.5, 44.5, 31.4, 30.2, 14.6, 14.2. MS: calcd m/z = 483.27; found m/z = 483.36.

The synthesis of BDPbiPh and BDPtriPh is similar to that of BDPmPh except that the ratio of BDP to 4-(diethylamino)benz-aldehyde was changed to 1 : 3 and 1 : 5, respectively. For BDPbiPh, yield: 23%. ^{1}H NMR ($CDCl_3$, 400 MHz): δ (ppm) 7.56–7.44 (m, 9H), 7.34–7.31 (m, 2H), 7.17 (d, J = 16.0 Hz, 4H), 6.68–6.58 (m, 6H), 3.41 (q, J = 6.8 Hz, 8H), 1.41 (s, 6H), 1.20 (t, J = 7.2 Hz, 12H). ^{13}C NMR (75 MHz, $CDCl_3$): δ (ppm) 152.77, 148.28, 140.69, 136.24, 135.89, 135.69, 132.89, 129.29, 128.82, 128.76, 128.54, 124.49, 117.10, 114.44, 111.51, 44.45, 14.47, 12.62. MS calcd m/z = 642.37; found m/z = 642.46. For BDPtriPh, yield: 12%. ^{1}H NMR ($CDCl_3$, 400 MHz): δ (ppm) 7.59–7.46 (m, 10H), 7.32–7.31 (m, 3H), 7.18 (d, J = 16.0 Hz, 3H), 6.69–6.59 (m, 9H), 3.41 (d, J = 6.0 Hz, 12H), 1.43 (s, 3H), 1.20 (t, J = 7.0 Hz, 18H). ^{13}C NMR (75 MHz, $CDCl_3$) δ (ppm) 195.56, 167.69, 161.64, 147.97, 139.81, 137.47, 137.30, 136.81, 136.77, 132.51, 131.01, 130.81, 130.12, 129.91, 128.77, 128.35, 125.72, 108.74, 68.14, 46.05, 39.29, 38.74, 29.64, 23.04, 13.99, 10.56. MS: m/z = 801.43; found m/z = 801.48.

Preparation of BDPmPh, BDPbiPh, and BDPtriPh nanoparticles

Nano-precipitation with DSPE-PEG$_{2000}$ was used to prepare nanoparticles of the three compounds. Taking BDPmPh as an example, a mixture of BDPmPh (10 mg) and DSPE-PEG$_{2000}$ (1 mg) was dissolved in tetrahydrofuran (THF, 1 mL) with ultrasound. Then 200 μL BDPmPh mixture (10 mg mL^{-1}) was added into distilled water (10 mL) under vigorous stirring at

room temperature. THF was removed by purging with nitrogen for 20 min. BDPmPh NPs in the solution were obtained by centrifugation.

Cell culture and MTT assay

HeLa cell lines were obtained from the Institute of Biochemistry and Cell Biology, SIBS, CAS (China). They were cultured in a medium consisting of DMEM (Dulbecco's modified Eagle's medium, Gibco) and 10% FBS (fetal bovine serum) at 37 °C under an atmosphere of 5% CO_2. The nanoparticles of the three compounds were first dissolved in phosphate buffered saline (PBS) and diluted with DMEM to various concentrations in 96-well plates. These 96-well plates were irradiated with a laser (1 W cm^{-2}) (660 nm for BDPmPh NPs, 730 nm for BDPbiPh NPs, and 808 nm for BDPtriPh NPs). Cell viability was determined by the MTT (3-(4,5-dimethylthiazol-2-yl)-2,5-diphenyltetrazolium bromide) assay. A solution of MTT (5 mg mL^{-1}, 20 μL) was added to each well after incubation for 4 h under the same conditions at 37 °C. Then the liquid was discarded, followed by the addition of 150 μL of DMSO. The absorbance (at 492 nm) of the solutions in the plates was measured on a reader at room temperature (BioTek microplate reader). The cell viability was then determined by the following equation: viability (%) = mean absorbance in each group incubated with different concentrations of corresponding NPs/mean absorbance in the control group × 100%.

Cellular uptake, trypan blue staining, fluorescence imaging of cellular ROS and sub-cellular co-localization

HeLa cells were incubated with BDPmPh, BDPbiPh and BDPtriPh NPs at their corresponding IC$_{50}$ in confocal dishes for 24 h. Then these NP solutions were discarded and the cells were washed with PBS (3 mL), followed by treating with 1 mL poly-oxymethylene for 25 min. Polyoxymethylene was discarded and the cells were washed with PBS three times (1 mL). The three samples were further incubated with 2,7-dichlorodihydro-fluorescein diacetate (DCF-DA, 10 μmol) for another 3 min, and washed with PBS three times (1 mL). These samples were irradiated using the corresponding laser (1 W cm^{-2}) for 3 minutes. Fluorescence images were observed using an Olympus IX 70 inverted microscope. The samples incubated with DCF-DA under irradiation were excited with a 488 nm laser and fluorescence was recorded from 490 to 600 nm. HeLa cells were incubated with BDPmPh, BDPbiPh and BDPtriPh NPs for 24 h in a 96-well plate and irradiated with a laser (1 W cm^{-2}). After 1 h, DMEM was discarded and the cells were washed with PBS three times. Then these cells were treated with a trypan blue solution (1 μg mL^{-1}, 100 μL) for 8 min and observed using a microscope.

In vivo tumor treatment histology examination and fluorescence imaging

Animal ethics approval was obtained from the Animal Center of Nanjing Medical University (NJMU, Nanjing, China) for this study (SCXK-2012-004). 35 nude mice were injected in the armpit with HeLa cells as the tumor source. When the tumor

volume reached about 100 mm^3, the mice were divided into 7 groups randomly. Mice in the control group were intravenously injected with saline and those in the illumination groups were intravenously injected with BDPmPh (100 μg mL^{-1}, 100 μL), BDPbiPh (100 μg mL^{-1}, 100 μL) and BDPtriPh NPs (100 μg mL^{-1}, 100 μL) in PBS solution. After 24 h, the tumors of the control and illumination groups were irradiated using a laser (BDPmPh NPs: 660 nm, 1 W cm^{-2}. BDPbiPh NPs: 730 nm, 1 W cm^{-2}. BDPtriPh NPs: 808 nm, 1 W cm^{-2}) for 8 minutes while the mice in the groups without illumination were not irradiated exceptionally. The body weights and tumor volumes of these mice were recorded every two days. After treatment, these nude mice were sacrificed. The tumors and main organs (heart, liver, spleen, lungs and kidneys) were analyzed by histology. The tissues of the tumors and main organs were embedded in paraffin cassettes and stained with hematoxylin and eosin (H&E) after dehydration, and the images were recorded on a microscope.

Results and discussion

The synthesis of BDPmPh, BDPbiPh and BDPtriPh is shown in Fig. S1.† Generally, by changing the ratio between (5,5-difluoro-1,3,7,9-tetramethyl-10-phenyl-5*H*-dipyrrolo[1,2-*c*:2′,1′-*f*][1,3,2] diazaborinin-4-ium-5-uide) and 4-(diethylamino)benzaldehyde (1 : 2.2, 1 : 3 and 1 : 5), BDPmPh, BDPbiPh and BDPtriPh can be obtained in the presence of acetic acid and piperidine with the protection of N$_2$. Their chemical structures have been fully characterized by ^{1}H NMR, ^{13}NMR and mass spectrometry (Fig. S2–S7†). The three compounds exhibit peaks at 565 and 611 nm for BDPmPh, 644 and 704 nm for BDPbiPh, and 647 and 758 nm for BDPtriPh, (Fig. 1a). The absorption peaks of these compounds red shift to the longer NIR region with the increase of the number of diethylamino groups introduced onto the BODIPY core, owing to the larger conjugated system. To improve the water dispersity of the compounds, 1,2-distearoyl-*sn*-glycero-3-phos-phoethanolamine-*N*-[amino(polyethylene glycol)$_{2000}$] (DSPE-PEG$_{2000}$) was used to prepare the nanoparticles (NPs) of these compounds by nanoprecipitation. As shown in Fig. 1b, the NPs of BDPmPh and BDPbiPh exhibit peaks at 568 and 619 nm, and 683 and 735 nm, respectively, while for the BDPtriPh NPs, the peaks become broader than those in THF (peaks at 683 and 759 nm), indicating the aggregation of these compounds.

To investigate the effect of pH on absorbance, the spectra were recorded in PBS at a pH of 5.5. Slight red shifting of the absorption peaks of these NPs was observed (BDPmPh NPs: 572 and 626 nm, BDPbiPh NPs: 689 and 738 nm, and BDPtriPh NPs: 694 and 776 nm). In the photoluminescence (PL) spectra, BDPmPh, BDPbiPh and BDPtriPh show emission with maximum intensity at 651 and 710 nm, 767 and 801 nm and 745 and 814 nm, respectively (Fig. 1c). Similarly, for the NPs of the compounds in PBS (pH 7.4), their emission moves to longer wavelengths. It can be seen that with diethylamino groups as the proton acceptor, red shifting was also observed in PBS (pH 5.5) (Fig. 1d). Singlet oxygen generation is crucial for a photosensitizer used as a phototherapy agent. The pH triggered generation of singlet oxygen was measured using DPBF
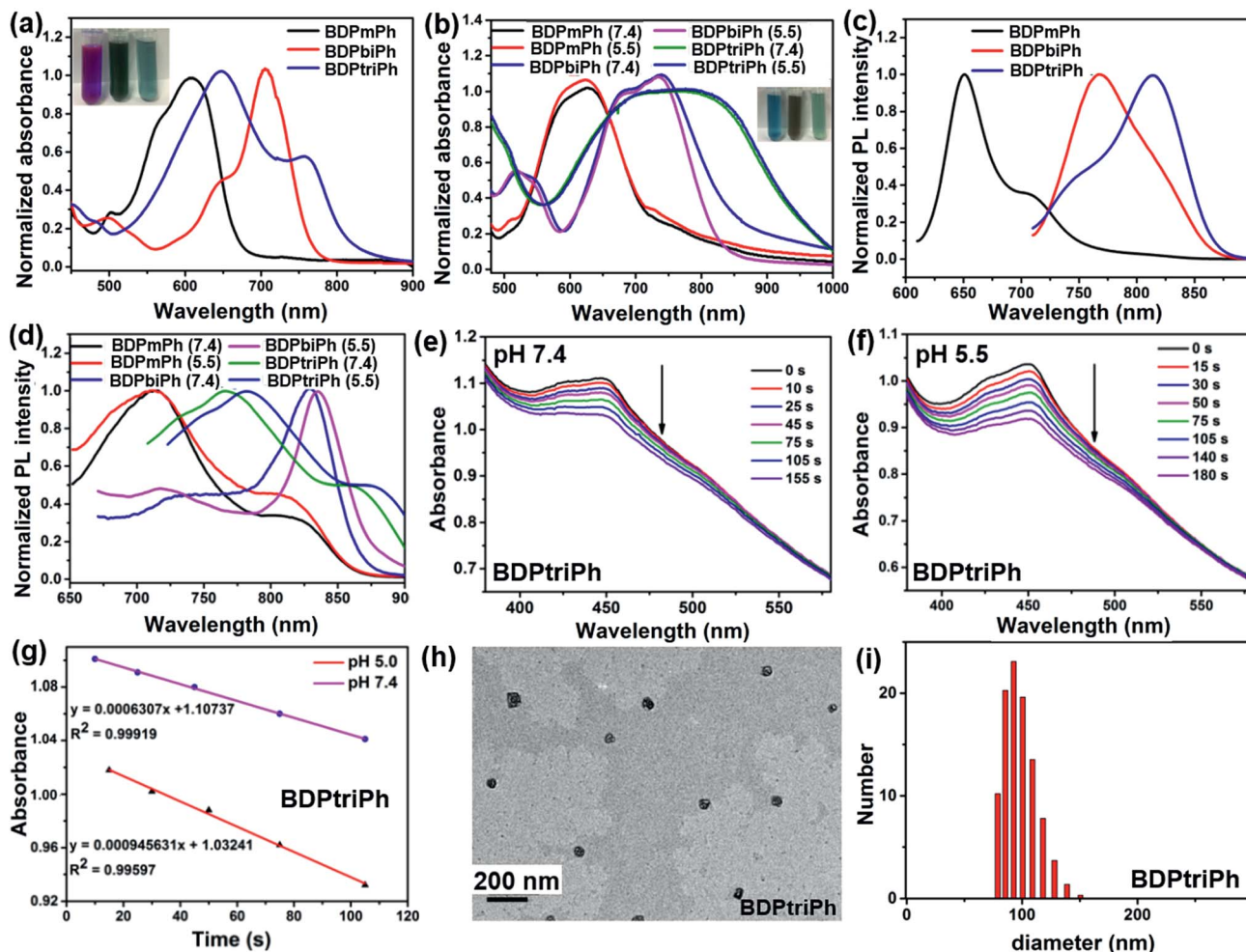
Fig. 1 (a) Normalized absorbance spectra and pictures of BDPmPh, BDPbiPh and BDPtriPh in THF. (b) Normalized absorbance spectra and pictures of the NPs in PBS at different pH (7.4 and 5.5). (c, d) Normalized PL spectra of the NPs in THF and of the corresponding NPs in PBS (pH 7.4 and 5.5). (e, f) Degradation of DPBF in the presence of the BDPtriPh NPs in PBS (pH 7.4 and 5.5). (g) Linear fitting of the degradation data of DPBF at different pH. (h, i) TEM image and DLS results of the BDPtriPh NPs.

(1,3-diphenylisobenzofuran) as the $^1O_2$ indicator. The absorbance of DPBF was adjusted to around 1.0 while that of the NPs was around 0.2 to 0.3. After exposing the mixture of these NPs and DPBF in PBS to different pH, the spectra were recorded. As shown in Fig. S8, S9,† 1e and g, the degradation of DPBF in low pH (5.5) was accelerated compared with that in high pH (7.4), which was confirmed by the linear fitting slope of the degradation. It can be concluded that these three NPs show superior singlet oxygen generation under acidic conditions, which may enhance the photodynamic therapy efficacy. To characterize the morphology and size of the BDPmPh, BDPbiPh and BDPtriPh NPs, transmission electron microscopy (TEM) and dynamic light scattering (DLS) have been applied. As illustrated in Fig. S10,† 1h and i, the TEM images of the BDPmPh, BDPbiPh and BDPtriPh NPs showed a well dispersed spherical morphology with a hydrodynamic size distribution from 52 to 172 nm, 78 to 200 nm and 82 to 152 nm, respectively, in accordance with the size demonstrated by DLS. These NPs possess suitable sizes for potential passive targeting by the enhanced permeability and retention effect.

pH triggered photothermal conversion and photostability of the nanoparticles

To investigate the photothermal conversion ability of the BDPmPh, BDPbiPh and BDPtriPh NPs, their photothermal conversion efficiency were measured. As shown in Fig. 2a, the BDPmPh, BDPbiPh and BDPtriPh NPs (100 μg mL^{-1}) were irradiated with 660, 730 and 808 nm lasers (1 W cm^{-2}) for 12 min and cooled to room temperature, respectively. While that of water is almost negligible, the temperature elevations of these three NPs are 12.5, 19.5 and 35.1 °C, respectively. From Fig. 2c and S11a and b,† it can be observed that the photothermal conversion efficiencies of these NPs are 27.3%, 37.9% and 60.5%, respectively.

Enhanced photothermal conversion efficiency can be detected when more diethylamino groups are introduced onto the BDP core. To further investigate the effect of pH on the photothermal efficiency of such NPs, the temperature changes of these NPs were recorded at the same concentration in PBS (pH 5.5). Fig. S11c, 11d† and 2e show that when exposed to PBS
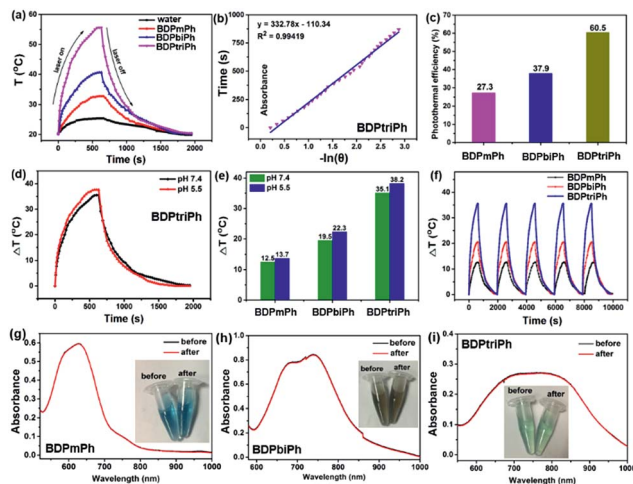
Fig. 2 (a) Temperature elevation of water and the BDPmPh, BDPbiPh and BDPtriPh NPs during irradiation for 12 min and cooling to room temperature. (b) Linear fitting of $-\ln \theta$ and time in the cooling curve of the BDPtriPh NPs. (c) Photothermal conversion efficiency of the BDPmPh, BDPbiPh and BDPtriPh NPs. (d) Temperature elevation of the BDPtriPh NPs in PBS at different pH. (e) Temperature changes of the BDPmPh, BDPbiPh and BDPtriPh NPs at different pH (7.4 and 5.5). (f) Temperature change of these NPs after irradiation and cooling for 5 cycles. Photo of (g) BDPmPh (h) BDPbiPh and (i) BDPtriPh NPs in water before and after irradiation.

media with a lower pH, the BDPmPh, BDPbiPh and BDPtriPh NPs exhibit superior temperature elevations of 13.7, 22.3 and 38.2 °C (Fig. 2e), respectively. It can be concluded that the lower pH further contributes to the photothermal conversion ability of these NPs.

To explain this phenomenon, it is assumed that the pH-sensitive property of the BDPmPh, BDPbiPh and BDPtriPh NPs arises from the photoinduced electron transfer (PET) mechanism, as illustrated in Scheme 1. Diethylamino (–NEt$_2$)

groups can serve as the proton acceptors because they can be protonated in PBS with weak acidity. According to the Jablonski diagram, the photon-excited electron can go back to the ground state (S$_0$) through vibrational relaxation or radioactive relaxation, which leads to fluorescence emission or the thermal effect, respectively.[35] It is also possible for an excited electron to enter the triplet state through intersystem crossing (ISC), which, in turn, triggers a photochemical reaction to produce reactive oxygen species (ROS).

Under neutral conditions, the HOMO level of the -NEt$_2$ group is between the HOMO and the LUMO levels of the photosensitizer. Consequently, the –NEt$_2$ groups transfer an electron to the HOMO of the photosensitizer after excitation while the excited electron of the photosensitizer tends to be shunted to the HOMO of the –NEt$_2$ group rather than undergoing ISC or radioactive or vibrational relaxation. Under acidic conditions, the H$^+$ bonded –NEt$_2$ group makes its HOMO lower than that of the photosensitizer and therefore, it can turn on the photothermal and photodynamic behavior of the photosensitizer. It may also be assumed that the more –NEt$_2$ groups the BDP derivatives have, the higher photothermal conversion efficiency the BDP derivatives will show because more –NEt$_2$ groups can be protonated when exposed to acidic conditions, which is consistent with the results above.

Since the photostability of the photosensitizers plays a major role in phototherapy, the photostability of the BDPmPh, BDPbiPh, and BDPtriPh NPs was evaluated (Fig. 2f). The temperature increase of these three NPs shows no obvious decrease after irradiation for 5 cycles (BDPmPh: 660 nm, 1 W cm^{-2}; BDPbiPh: 730 nm, 1 W cm^{-2}; BDPtriPh: 808 nm, 1 W cm^{-2}). After irradiation, the absorbance of these three NPs was measured. As shown in Fig. 2g–i, no significant changes were detected in the absorbance, indicating their outstanding ability to resist photobleaching.
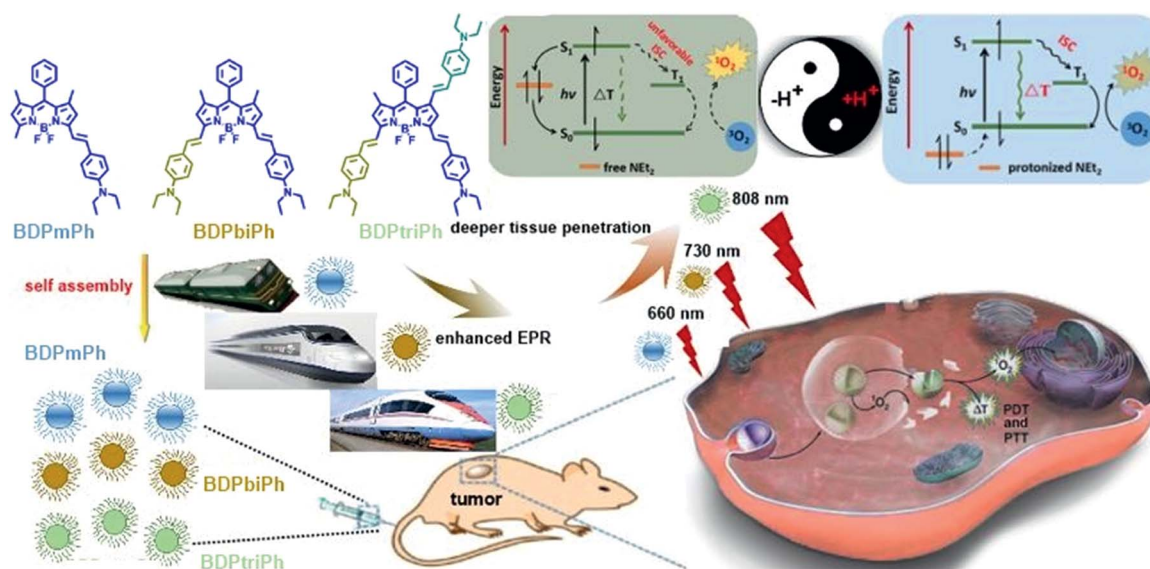
Scheme 1 Illustration of the preparation and application of the BDPmPh, BDPbiPh and BDPtriPh NPs and the mechanism of pH triggered NPs for enhanced PDT/PTT.

MTT assay, trypan blue staining, cellular uptake and sub-cellular organelle co-localization

Ideal photosensitizers should possess high phototoxicity upon light irradiation and low dark toxicity for phototherapy. To evaluate the toxicity of the BDPmPh, BDPbiPh and BDPtriPh NPs, MTT assays were performed. As shown in Fig. S12† and 3a, these three NPs show negligible dark toxicity because the cell viability remains at a high level in each group without light irradiation. In contrast, high phototoxicity causes a dramatic decrease in cell viability upon light irradiation (BDPmPh, 660 nm, 1 W cm^{-2}, BDPbiPh, 730 nm, 1 W cm^{-2}, and BDPtriPh, 808 nm, 1 W cm^{-2}). For the BDPmPh NPs, the half-maximal inhibitory concentration (IC$_{50}$) is approximately 59.06 μM, while that of the BDPbiPh NPs is 22.40 μM. For the BDPtriPh NPs, the lowest IC$_{50}$ is only 4.16 μM (Fig. 3b). To further confirm the phototherapy efficiency of these NPs, trypan blue staining was employed. Fig. 3c shows that in the control group (without the NPs), HeLa cells remained alive, regardless of light irradiation. When HeLa cells were cultured with the BDPmPh, BDPbiPh and BDPtriPh NPs for 24 h in the dark, the cells still remained alive as only a few cells can be stained in blue, indicating low dark toxicity of these NPs. As indicated by the homogeneous blue, the cells incubated with the NPs under light irradiation were substantially killed, suggesting high phototoxicity of these NPs. Confocal laser scanning microscopy (CLSM) was employed to investigate the cellular uptake of the BDPmPh, BDPbiPh and BDPtriPh NPs. As illustrated in Fig. 3d, these NPs can be taken up by HeLa cells effectively after incubation for 24 h, as demonstrated by the red colour. In addition, DCF-DA was used to detect the generation of singlet oxygen;

these NPs can generate singlet oxygen with light irradiation, indicating their potential phototherapy effect. Sub-cellular co-localization in lysosomes was investigated by a commercial probe-Lyso tracker green. Fig. 3e demonstrates that these NPs with red fluorescence exhibit excellent co-localization with the lysosomes with green fluorescence, indicating effective endocytosis. It is expected that once endocytosed, these NPs can show enhanced PDT and PTT *in vivo*.

Fluorescence and photothermal imaging guided PDT/PTT synergistic therapy

Since BDPmPh, BDPbiPh and BDPtriPh NPs are efficient for cancer ablation *in vitro*, to further study the phototherapy efficacy, three HeLa bearing nude mice were intravenously injected with the BDPmPh, BDPbiPh and BDPtriPh NPs (100 μg mL^{-1}, 100 μL), respectively. The fluorescence was recorded at different time. At the beginning (0 h), no obvious fluorescence could be detected. These NPs can accumulate in the tumor region gradually as shown by the increased fluorescence, which indicates the good EPR effect of these three NPs. However, the most suitable times for phototherapy of the BDPmPh and BDPbiPh NPs are 8 and 6 h after intravenous injection, respectively, when the fluorescence reached a maximum. However, for the BDPtriPh NPs, the time has been greatly decreased to only 4 h, indicating that BDPtriPh NPs have the best EPR efficiency. This may be explained by the fact that BDPtriPh with three diethylamino groups can accept the largest number of protons, which is vividly illustrated by the three Chinese trains in Scheme 1. Among the three trains, the "Fuxing (means renaissance) train" is the quickest (like the BDPtriPh NPs), the "Hexie
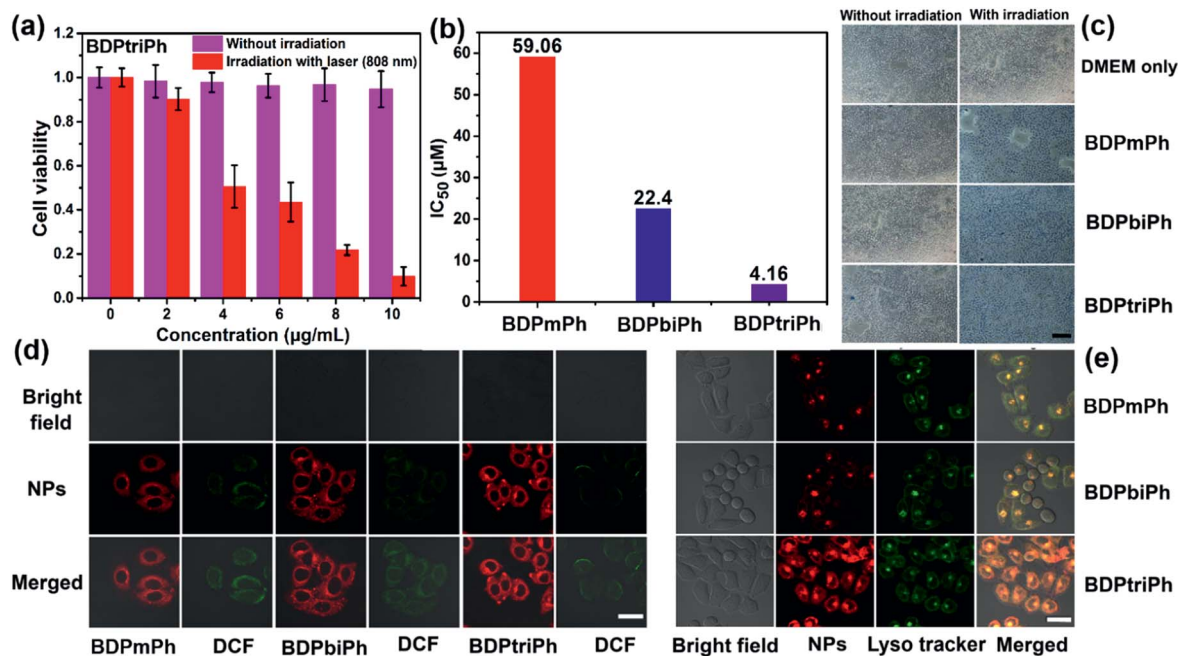

Fig. 3 (a) MTT assay results of BDPtriPh NPs with and without laser irradiation (808 nm, 1 W cm^{-2}) on HeLa cells. (b) IC$_{50}$ of the BDPmPh, BDPbiPh and BDPtriPh NPs. (c) Trypan blue stained Hela cells with and without laser irradiation; blue indicates dead cells. Scale bar: 25 μm. (d) Cellular uptake of the NPs and cellular ROS generation with DCF-DA as the probe. Scale bar: 10 μm. (e) Lyso tracker stained Hela cells, showing that the NPs can be located in the lysosomes. Scale bar: 10 μm.
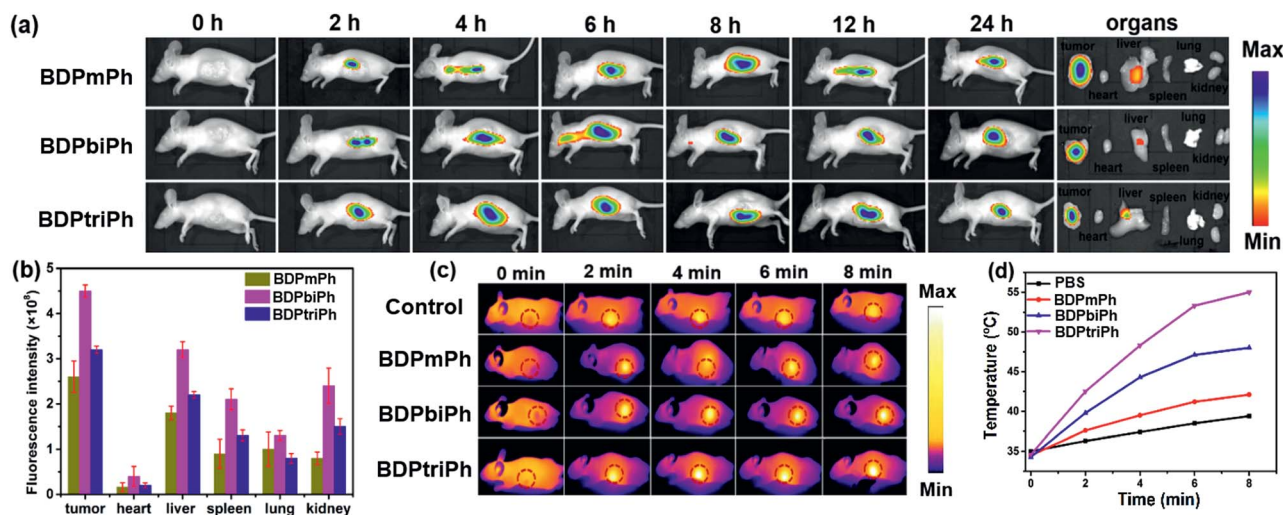
Fig. 4 (a) *In vivo* fluorescence imaging of nude mice with the BDPmPh, BDPbiPh and BDPtriPh NPs for different times and the bio-distribution of the NPs in the tumor, heart, liver, spleen, lungs and kidneys. (b) Fluorescence intensity of the NPs in the tumor and main organs 24 h after intravenous injection. (c) Pictures of nude mice after 8 min of irradiation (1 W cm^{-2}). (d) Temperature elevation of nude mice after intravenous injection of the BDPmPh, BDPbiPh and BDPtriPh NPs after 8 min of irradiation (1 W cm^{-2}).

"(means harmony) train" is a little slower (like the BDPbiPh NPs) while the "green train" is the slowest (like the BDPmPh NPs). 24 h after injection, these mice were sacrificed and the bio-distribution in the tumor, heart, liver, lungs, spleen and kidneys was recorded (three mice per group) by fluorescence imaging (Fig. 4b). The relative fluorescence intensities demonstrate that these NPs still accumulate in the tumor, followed by the liver and kidneys. To further investigate the photothermal effect of these NPs *in vivo*, the temperature was recorded after intravenous injection of the BDPmPh, BDPbiPh and BDPtriPh

NPs for 8, 6 and 4 h, respectively. A temperature elevation of 10.2, 15.2 and 23.5 °C could be observed for irradiation within 8 min, respectively (Fig. 4c), indicating their excellent phototherapy effect.

As shown by the change in tumor volume (Fig. 5a), after only three treatments, the tumors treated with the BDPtriPh NPs have disappeared, indicating the best efficacy, while the BDPmPh NPs (relative tumor volume is 0.42) and BDPbiPh NPs (relative tumor volume is 0.23) did not perform so well. However for the groups without irradiation, the tumor volume is similar
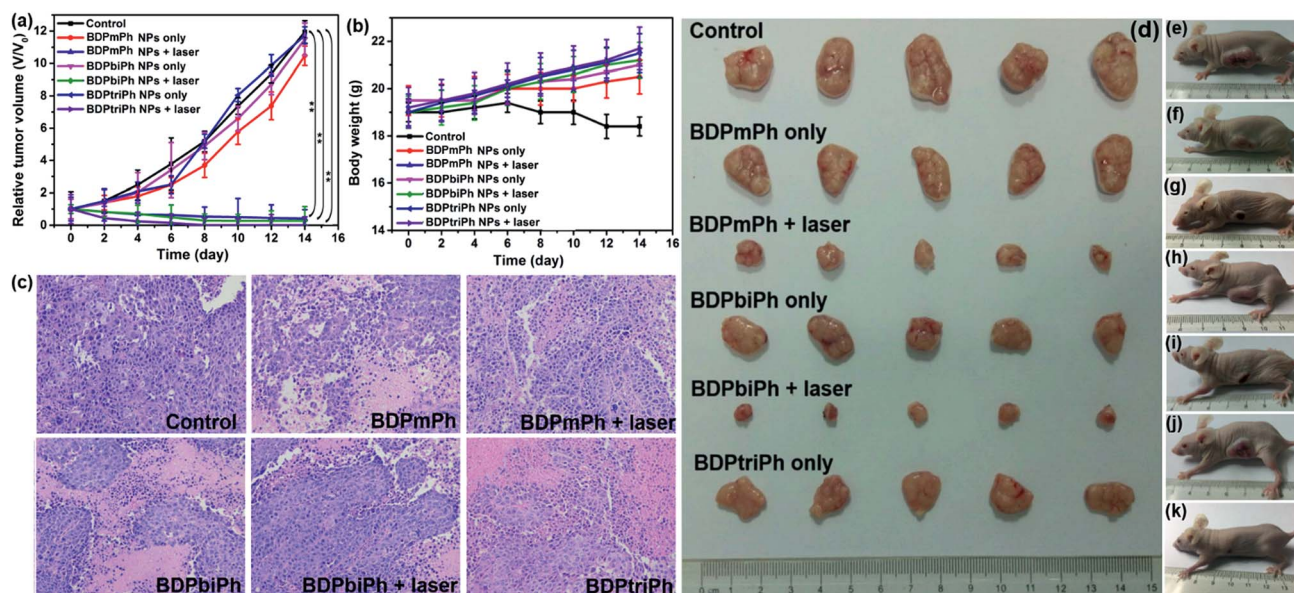

Fig. 5 (a) Relative tumor volume (**$p < 0.01$ compared with the control group) and (b) body weight change during the treatment. (c) Pictures of H&E stained tumors. Scale bar: 100 µm. (d) Illustration of the tumors in each group. (e–k) Pictures of the mice of the control, BDPmPh NP, BDPmPh NPs + laser, BDPbiPh NP, BDPbiPh NPs + laser, BDPtriPh NP and BDPtriPh NPs + laser groups.
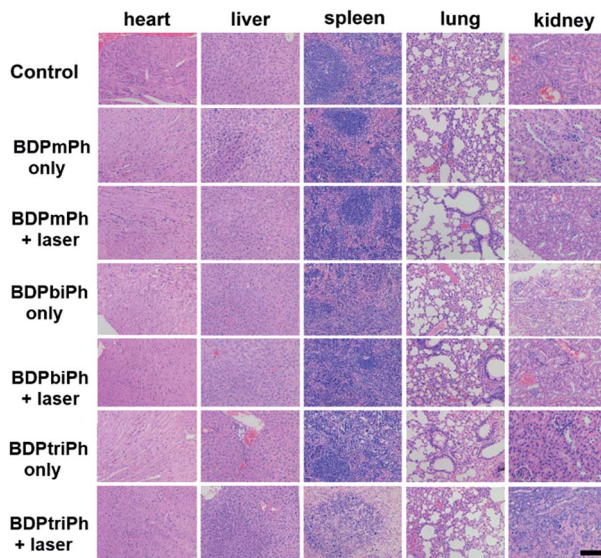
Fig. 6 Images of the H&E stained heart, liver, spleen, lungs, and kidneys after treatment. Scale bar: 100 μm.

to that of the control group, indicating the low dark toxicity of these NPs. The body weight measured every two days shows that the mice injected with the BDPmPh, BDPbiPh and BDPtriPh NPs became fat, suggesting the low dark toxicity of these NPs (Fig. 5b). The tumors of the mice after sacrifice are shown in Fig. 5d and the mice after treatment are shown in Fig. 5e–k.

To further evaluate the toxicity of these NPs, images of the H&E stained tumors were recorded. Fig. 5c shows that in the control groups and the ones without irradiation, the nuclei of the tumors are almost unchanged while parts of the nuclei are distorted and even destroyed in the irradiation groups. The images of the H&E stained main organs (heart, spleen, liver, lungs and kidneys) in Fig. 6 show that these NPs cause almost no damage to normal tissues, indicating the low dark toxicity, good phototoxicity and excellent bio-compatibility of these NPs and the best efficacy of the BDPtriPh NPs for the ablation of tumors.

Conclusions

In conclusion, wavelength-tunable BODIPY derivatives, BDPmPh, BDPbiPh and BDPtriPh, have been synthesized by the condensation of different numbers of diethylamino groups onto the BODIPY core. These compounds are sensitive to pH and can be activated by the acidity of lysosomes. DSPE-PEG$_{2000}$ coated NPs show enhanced singlet oxygen generation and photothermal conversion ability in low pH. With the increase of diethylaminophenyl groups conjugated with the BODIPY core, a longer NIR wavelength, a higher photothermal conversion, a better EPR effect, and better phototherapy efficacy can be obtained. The BDPtriPh NPs are the best theranostic agents for fluorescence and photothermal imaging guided PDT and PTT. This investigation offers a strategy to tune the photoconversion characteristics of fluorophore dyes for both wavelength and pH-dependent PDT/PTT synergistic cancer therapy.

Conflicts of interest

There are no conflicts to declare.

Acknowledgements

Notes and references

1 R. L. Siegel, K. D. Miller and A. J. DVM, *Ca-Cancer J. Clin.*, 2018, **68**, 7–30.
2 N. Shivran, M. Tyagi, S. Mula, P. Gupta, B. Saha, B. S. Patro and S. Chattopadhyay, *Eur. J. Med. Chem.*, 2016, **122**, 352–365.
3 M. Laine, N. A. Barbosa, A. Kochel, B. Osiecka, G. Szewczyk, T. Sarna, P. Ziółkowski, R. Wieczorek and A. Filarowski, *Sens. Actuators, B*, 2017, **238**, 548–555.
4 X. Song, Q. Chen and Z. Liu, *Nano Res.*, 2014, **8**, 340–354.
5 A. Carija, N. Puizina-Ivic, D. Vukovic, L. Miric Kovacevic and V. Capkun, *Photodiagn. Photodyn. Ther.*, 2016, **16**, 60–65.
6 A. Kamkaew, S. H. Lim, H. B. Lee, L. V. Kiew, L. Y. Chung and K. Burgess, *Chem. Soc. Rev.*, 2013, **42**, 77–88.
7 C. C. Chang, M. C. Hsieh, J. C. Lin and T. C. Chang, *Biomaterials*, 2012, **33**, 897–906.
8 J. Schmitt, V. Heitz, A. Sour, F. Bolze, H. Ftouni, J. F. Nicoud, L. Flamigni and B. Ventura, *Angew. Chem., Int. Ed.*, 2015, **54**, 169–173.
9 E. Secret, M. Maynadier, A. Gallud, A. Chaix, E. Bouffard, M. Gary-Bobo, N. Marcotte, O. Mongin, K. El Cheikh, V. Hugues, M. Auffan, C. Frochot, A. Morere, P. Maillard, M. Blanchard-Desce, M. J. Sailor, M. Garcia, J. O. Durand and F. Cunin, *Adv. Mater.*, 2014, **26**, 7643–7648.
10 M. Li, Y. Gao, Y. Y. Yuan, Y. Z. Wu, Z. F. Song, B. Z. Tang, B. Liu and Q. C. Zheng, *ACS Nano*, 2017, **11**, 3922–3932.
11 X. L. Cai, C. J. Zhang, F. T. W. Lim, S. J. Chan, A. Bandla, C. K. Chuan, F. Hu, S. D. Xu, N. V. Thakor, L. D. Liao and B. Liu, *Small*, 2016, **12**(47), 6576–6585.
12 B. B. Gu, W. B. Wu, G. X. Xu, G. X. Feng, F. Yin, P. H. Joo Chong, J. L. Qu, K. T. Yong and B. Liu, *Adv. Mater.*, 2017, **34**, 1701076.
13 J. F. Zhou, L. Z. Gai, Z. K. Zhou, W. Yang, J. Mack, K. J. Xu, J. Z. Zhao, Y. Zhao, H. L. Qiu, K. S. Chan and Z. Shen, *Chem.–Eur. J.*, 2016, **22**, 13201–13209.
14 S. H. Wang, L. Shang, L. L. Li, Y. J. Yu, C. W. Chi, K. Wang, J. Zhang, R. Shi, H. Y. Shen, G. I. N. e Waterhous, S. J. Liu, J. Tian, T. R. Zhang and H. Y. Liu, *Adv. Mater.*, 2016, **28**, 8379–8387.

15 S. D. Xu, Y. Y. Yuan, X. L. Cai, C. J. Zhang, F. Hu, J. Liang, G. X. Zhang, D. Q. Zhang and B. Liu, *Chem. Sci.*, 2015, **6**, 5824–5830.

16 R. Lincoln, L. Kohler, S. Monro, H. M. Yin, M. Stephenson, R. F. Zong, A. Chouai, C. Dorsey, R. Hennigar, R. P. Thummel and S. A. McFarland, *J. Am. Chem. Soc.*, 2013, **135**, 17161–171175.

17 G. R. Jin, G. X. Feng, W. Qin, B. Z. Tang, B. Liu and K. Li, *Chem. Commun.*, 2016, **52**, 2752–2755.

18 L. Y. Zeng, L. J. Luo, Y. W. Pan, S. Luo, G. M. Lu and A. G. Wu, *Nanoscale*, 2015, **7**, 8946–8954.

19 Y. C. Tsai, P. Vijayaraghavan, W. H. Chiang, H. H. Chen, T. I. Liu, M. Y. Shen, A. Omoto, M. Kamimura, K. Sog and H. C. Chiu, *Theranostics*, 2018, **8**, 1435–1447.

20 L. E. Zhang, L. Y. Zeng, Y. W. Pan, S. Luo, W. Z. Ren, A. Gong, X. H. Ma, H. Z. Liang, G. M. Lu and A. G. Wu, *Biomaterials*, 2015, **44**, 82–90.

21 J. H. Zou, Z. H. Yin, P. Wang, D. P. Chen, J. J. Shao, Q. Zhang, L. G. Sun, W. Huang and X. C. Dong, *Chem. Sci.*, 2018, **9**, 2188–2194.

22 J. H. Zou, Z. H. Yin, K. K. Ding, Q. Y. Tang, J. W. Li, W. L. Si, J. J. Shao, Q. Zhang, W. Huang and X. C. Dong, *ACS Appl. Mater. Interfaces*, 2017, **9**, 32475–32481.

23 M. Yu, F. Guo, J. Wang, F. Tan and N. Li, *ACS Appl. Mater. Interfaces*, 2015, **7**, 17592–17597.

24 Z. Hou, K. Deng, C. Li, X. Deng, H. Lian, Z. Cheng, D. Jin and J. Lin, *Biomaterials*, 2016, **101**, 32–46.

25 J. Cao, H. An, X. Huang, G. Fu, R. Zhuang, L. Zhu, J. Xie and F. Zhang, *Nanoscale*, 2016, **8**, 10152–10159.

26 P. Huang, J. Lin, S. Wang, Z. Zhou, Z. Li, Z. Wang, C. Zhang, X. Yue, G. Niu, M. Yang, D. Cui and X. Chen, *Biomaterials*, 2013, **34**, 4643–4654.

27 X. Tan, J. Wang, X. Pang, L. Liu, Q. Sun, Q. You, F. Tan and N. Li, *ACS Appl. Mater. Interfaces*, 2016, **8**, 34991–35003.

28 S. Gao, L. Zhang, G. Wang, K. Yang, M. Chen, R. Tian, Q. Ma and L. Zhu, *Biomaterials*, 2016, **79**, 36–45.

29 U. S. Chung, J. H. Kim, B. Kim, E. Kim, W. D. Jang and W. G. D. Koh, *Chem. Commun.*, 2016, **52**, 1258–1261.

30 D. Chen, C. Wang, X. Nie, S. Li, R. Li, M. Guan, Z. Liu, C. Chen, C. Wang and C. Shu, *Adv. Funct. Mater.*, 2014, **24**, 6621–6628.

31 H. Xiao, B. Zhu, D. Wang, Y. Pang, L. He, X. Ma, R. Wang, C. Jin, Y. Chen and X. Zhu, *Carbon*, 2012, **50**, 1681–1689.

32 G. Song, J. Hao, C. Liang, T. Liu, M. Gao, L. Cheng, J. Hu and Z. Liu, *Angew. Chem., Int. Ed.*, 2016, **55**, 2122–2126.

33 L. Huang, Z. J. Li, Y. Zhao, J. Y. Yang, Y. C. Yang, A. I. Pendharkar, Y. W. Zhang, S. Kelmar, L. Y. Chen, W. T. Wu, J. Z. Zhao and G. Han, *Adv. Mater.*, 2017, **29**, 1604789.

34 H. He, S. S. Ji, Y. He, A. J. Zhu, Y. L. Zou, Y. B. Deng, H. T. Ke, H. Yang, Y. L. Zhao, Z. Q. Guo and H. B. Chen, *Adv. Mater.*, 2017, **29**, 1606690.

35 Q. Y. Tang, W. Y. Xiao, C. H. Huang, W. L. Si, J. J. Shao, W. Huang, P. Chen, Q. Zhang and X. C. Dong, *Chem. Mater.*, 2017, **29**, 5216–5222.